Editors' Suggestion

Specific Heat of Electron Plasma Waves

J. R. Rygg,[1,2,3,*] P. M. Celliers,[4] and G. W. Collins[1,2,3]
[1]Laboratory for Laser Energetics, University of Rochester, Rochester, New York 14623, USA
[2]Department of Mechanical Engineering, University of Rochester, Rochester, New York 14623, USA
[3]Department of Physics and Astronomy, University of Rochester, Rochester, New York 14623, USA
[4]Lawrence Livermore National Laboratory, Livermore, California 94551, USA

(Received 25 October 2022; revised 31 March 2023; accepted 7 April 2023; published 31 May 2023)

Collective modes in a plasma, like phonons in a solid, contribute to a material's equation of state and transport properties, but the long wavelengths of these modes are difficult to simulate with today's finite-size quantum simulation techniques. A simple Debye-type calculation of the specific heat of electron plasma waves is presented, yielding up to $0.05k/e^-$ for warm dense matter (WDM), where thermal and Fermi energies are near 1 Ry = 13.6 eV. This overlooked energy reservoir is sufficient to explain reported compression differences between theoretical hydrogen models and shock experiments. Such an additional specific heat contribution refines our understanding of systems passing through the WDM regime, such as the convective threshold in low-mass main-sequence stars, white dwarf envelopes, and substellar objects; WDM x-ray scattering experiments; and the compression of inertial confinement fusion fuels.

DOI: 10.1103/PhysRevLett.130.225101

Specific heat is a measure of the energy per unit of substance required to produce a unit change of temperature. Specific heat plays a central role in thermodynamics and material properties such as compressibility, sound speed, viscosity, thermal diffusivity, and convective transport. In a microscopic picture, specific heat is related to the number of degrees of freedom of the constituent particles, and each available degree of freedom has a nominal heat capacity of $k/2$, where the Boltzmann constant $k = 1.380\,649 \times 10^{-23}\ \mathrm{J\,K^{-1}}$.

Early work by Debye [1] produced a compelling description of specific heat in solids through a quantum statistical treatment of long-range correlations between the ions, i.e., phonons. This model captures the essential behavior of specific heat at low temperatures by integrating the occupied density of phonon states and is still in wide use a century later.

In fluids, long-range correlations play a diminished role, so the phonon model is often dropped in favor of an ideal-gas model plus virial and other modifications [2]. Collective behavior reemerges in plasmas due to long-range electromagnetic interactions between the constituent charged particles. However, in the ideal plasma limit, the accessible collective modes with wavelengths shorter than the screening length are severely restricted; instead, the ideal gas is modified by exchange interactions and static local-field corrections [3]. Many-body contributions to the specific heat have long been a challenge to calculate accurately and offer particular challenges in the moderately coupled, partially degenerate warm-dense-matter (WDM) regime [4].

In this Letter, we present a simple model to identify the conditions where collective plasma oscillations contribute to the thermodynamics of the system. In particular, we focus on hydrogen in the WDM regime, although the results generalize to plasmas of any composition and thermodynamic condition. In warm dense hydrogen, several energy scales are simultaneously and approximately equal (Fig. 1), including (i) the hydrogen atom binding energy $1\ \mathrm{Ry} = \hbar^2/(2m_e a_0^2) = 13.6$ eV; (ii) the electron Fermi energy $E_F = [\hbar^2/(2m_e)](3\pi^2 n_e)^{2/3}$; (iii) the Coulomb coupling energy $E_C = e^2/(4\pi\varepsilon_0 a_s)$, where $a_s = (4\pi n_e/3)^{-1/3}$ is the electron sphere radius; (iv) the electron plasma oscillation energy $\hbar\omega_p = \hbar[n_e e^2/(\varepsilon_0 m_e)]^{1/2}$; and (v) the thermal energy kT.

Hydrogen has the simplest atomic structure and ionization state histogram, making it an excellent system to evaluate the contribution of plasma oscillations to the thermodynamic state. These oscillations have been experimentally observed in deuterium (^{2}H) shocked to WDM states [7,8] as well as other WDM systems [9–11]. Furthermore, recent deuterium shock experiments in the vicinity of $kT = E_F = 1$ Ry report evidence for increased compression compared to all theoretical models [5], consistent with an overlooked energy contribution.

Following the Debye model for phonons in a solid [1], we compute the internal energy content of longitudinal

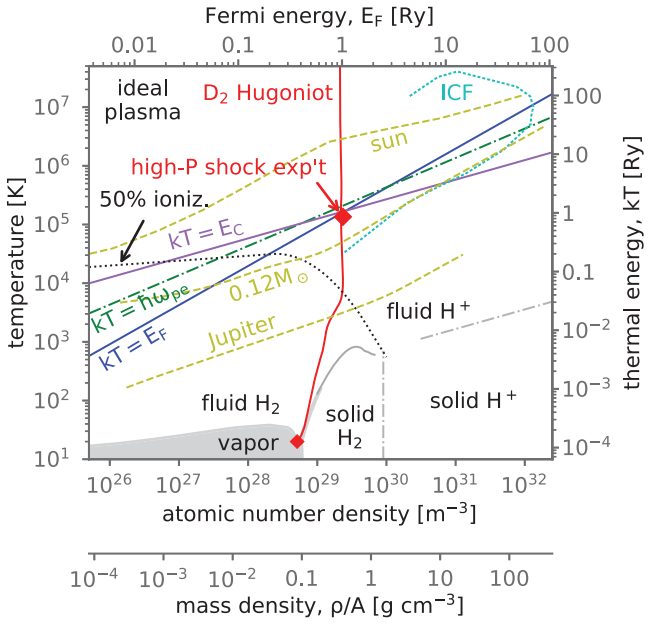

FIG. 1. Hydrogen density-temperature diagram. High-pressure shock experiments in deuterium [5] reach higher compression than predicted by theoretical models (solid red line; also see Fig. 4). This occurs in the warm-dense-matter regime where the thermal energy kT is approximately and simultaneously equal to (i) the isolated-atom binding energy (1 Ry = 13.6 eV), (ii) the Fermi energy E_F (assuming full ionization), (iii) the electron plasmon energy $\hbar\omega_p$, and (iv) the Coulomb coupling energy E_C. Also shown are the standard solar model, a main-sequence star with $M = 0.12M_\odot$, the pure-H Jupiter isentrope, and the dense fuel trajectory in an ignited inertial confinement fusion (ICF) implosion (experiment N210808 [6]).

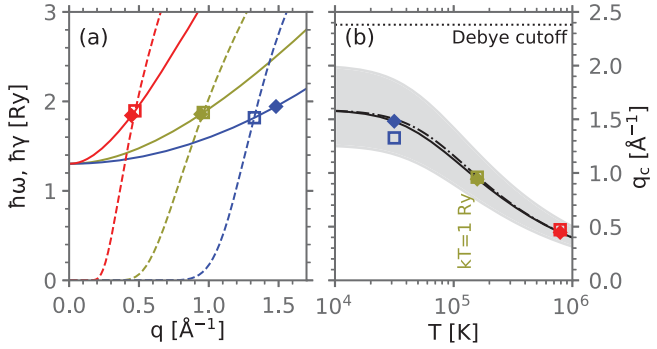

FIG. 2. For electron density $n_e = 2.3 \times 10^{29}$ m^{-3} ($E_F = 1$ Ry): (a) dispersion relation (solid lines) and damping rate (dashed lines) of electron plasma waves at $kT = (0.2, 1, \text{and } 5)$ Ry $= (32, 158, 790)$ kK in blue, yellow, and red, respectively; (b) screening cutoff wave number for $\zeta = 1$ (solid curve), its approximation using Eq. (3) (dash-dotted curve), and for $\zeta = 2^{\pm 1/3}$ (shaded gray region). Diamonds (open squares) show the screening (damping) cutoff wave numbers for the three temperature cases. Also shown is the Debye phonon model cutoff for solids (dotted black line).

electrostatic plasma oscillations (plasmons) as the integral (in our case, over wave number q) of the wave energy $\epsilon(q)$, the density of states $g(q)$, and the occupancy factor $f(q)$: $E_w = \int_0^{q_c} \epsilon(q) g(q) f(q) dq$. The integral is cut off at some maximum wave number q_c, above which the wavelength becomes too short to support collective oscillations, directly analogous to the Debye frequency for phonons in solids.

The density of states in a 3D volume V is approximated as in the Debye method: $g(q) = Vq^2/(2\pi^2)$. For electrostatic plasma waves, we have only a longitudinal component; the two transverse polarizations of phonons in solids are not present, and so too the extra factor of 3 in the density of states [1] is omitted.

We take the occupancy factor f to be the Bose-Einstein distribution function and assume zero chemical potential for the plasma waves: $f(q) = (e^{\hbar\omega_q/kT} - 1)^{-1}$, where we have replaced the wave energy with a dispersion relation, $\epsilon(q) = \hbar\omega_q$. Putting it all together, we get the plasma wave contribution to the internal energy:

$$E_w = \frac{V}{2\pi^2} \int_0^{q_c} \hbar\omega_q \frac{q^2 dq}{e^{\hbar\omega_q/kT} - 1}. \tag{1}$$

We may separately evaluate the internal energy contributions from the low-frequency ion-acoustic waves (IAWs) and the high-frequency electron plasma waves (EPWs, also known as Langmuir waves, plasmons). We will restrict our consideration to the case of longitudinal oscillations in a nonrelativistic ($kT, E_F \ll m_e c^2$), unmagnetized ($B \to 0$) material. We allow arbitrary electron degeneracy and neglect the radiation field. When ions and electrons are in thermal equilibrium, as is expected in many astrophysical objects and in shocks at high density, the IAWs experience critical damping on the ion thermal distribution for conditions throughout the WDM regime; we thus consider only the EPW modes for this analysis.

The EPW dispersion relation for full and arbitrary electron degeneracy has been reported elsewhere [12–18]. Here, we write the EPW dispersion relation as [see Fig. 2(a)]

$$\omega_q^2 = \omega_p^2 [1 + (q\lambda_E)^2] + \hbar^2 q^4/(4m_e^2), \tag{2}$$

where λ_E is the effective electron screening length.

Detailed expressions for the electron screening length at arbitrary electron degeneracy have been reported previously [16–18]. A convenient analytic approximation is given by [16] [see Fig. 2(b)]

$$\lambda_E^2 = 3\lambda_D^2 [1 + (2\Theta/5)^2]^{1/2}, \tag{3}$$

where $\lambda_D = [\varepsilon_0 kT/(n_e e^2)]^{1/2}$ is the Debye-Hückel electron screening length and $\Theta = E_F/(kT)$ is the quantum degeneracy parameter [19].

We now turn to the upper integration limit or cutoff wave number q_c. In the Debye phonon model [1], the model is normalized to reach the Dulong-Petit value of $C_V = 3k$ per atom at high temperatures by introducing an *ad hoc* cutoff

at a maximum wave number $q_D = (6\pi^2 n_i)^{1/3}$. This Debye cutoff is related to the Debye frequency or Debye temperature through the sound speed c_s, namely, $\hbar c_s q_D = \hbar\omega_D = kT_D$. A cubic volume corresponding to this minimum wavelength, $V = (2\pi/q_D)^3$, contains $4\pi/3 \approx 4.19$ atoms.

For plasmons, we expect an effective cutoff when either (i) the wave number exceeds the inverse screening length or (ii) the damping rate exceeds the oscillation frequency, where the damping rate for EPWs with arbitrary degeneracy has been reported previously [e.g., Refs. [13,16–18]; see Fig. 2(a)]. We can map the critical damping condition (ii) onto the critical screening condition (i) through the dispersion relation of Eq. (2) and defining the cutoff wave number as a scalar divided by the screening length:

$$q_c = \zeta/\lambda_E. \tag{4}$$

Figure 2(b) shows that at $E_F = 1$ Ry these two cutoff conditions are nearly coincident with $\zeta = 1$. In the WDM regime, this wave number cutoff is always smaller than the Debye phonon cutoff; for example, at $kT = E_F = 1$ Ry, the cubic volume corresponding to the cutoff contains 62.2 electrons, about 15 times as many particles as the Debye phonon cutoff of 4.19.

Integration of Eq. (1) with the EPW dispersion and cutoff gives the internal energy of the electron plasma waves E_w. Isochoric heat capacity $C_V = (\partial E_w/\partial T)_V$. Figure 3 shows the results for $\zeta = 1$ over a wide range of density-temperature space, with lineouts along the isochore corresponding to $E_F = 1.0$ Ry. The shaded region corresponds to a range of $\zeta = 2^{\pm 1/3}$, a factor of 2 in the cutoff screening volume. Detailed consideration of additional effects that were neglected here, such as subcritical damping, collisions, local field corrections, partial ionization, and higher-order terms in the dispersion relation, are not expected to extend beyond this range.

An approximate algebraic expression for the energy integral can be obtained by assuming the EPW frequency does not depend on the wave number. Defining $\Omega = (1+\zeta^2)^{1/2}[\hbar\omega_p/(kT)]$, the EPW internal energy can be approximated as [20]

$$\frac{E_w}{NkT} \approx \frac{\zeta^3}{6\pi^2 n_e \lambda_E^3} \frac{\Omega}{e^\Omega - 1}, \tag{5}$$

where N is the number of electrons. The corresponding explicit form for the specific heat is [20]

$$\frac{C_V}{Nk} \approx \frac{E_w}{NkT}\left[\frac{\Omega}{1-e^{-\Omega}} - \frac{3}{2} + \frac{(6/25)\Theta^2}{1+(4/25)\Theta^2}\right]. \tag{6}$$

This approximation tracks closely with the full integral for both energy and specific heat (Fig. 3) and falls within the $\zeta = 2^{\pm 1/3}$ range. Integral and algebraic expressions for the corresponding EPW pressure contribution can be found in Supplemental Material [20].

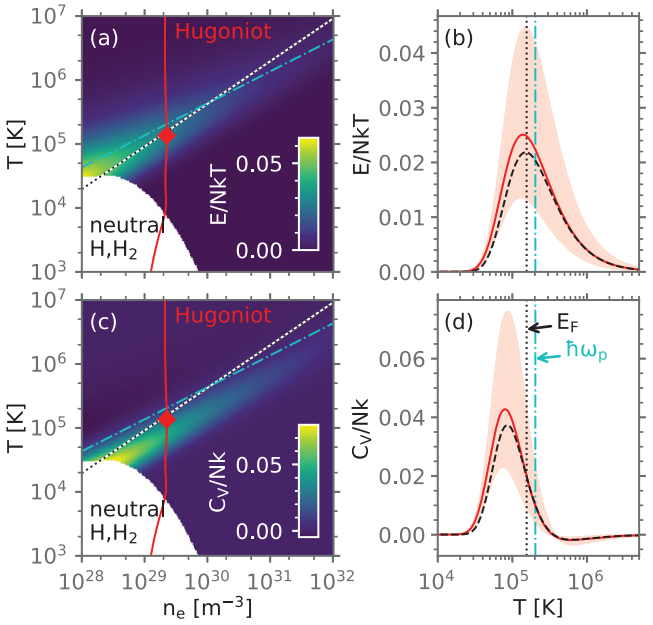

FIG. 3. (a),(b) Internal energy and (c),(d) isochoric heat capacity contributions of electron plasma waves. (a),(c) Contours of $E_F = kT$ and $\hbar\omega_p = kT$ are shown as dotted and dashed-dotted lines, respectively. The hydrogen shock Hugoniot starting from cryogenic liquid is in solid red, with a red diamond for the highest-pressure shock experiment that observed enhanced compression compared to theory [5]. (b),(d) Temperature lineouts (solid red line) are at $n_e = 2.2 \times 10^{29}$ m^{-3} ($E_F = 0.98$ Ry), corresponding to the density of these shock experiments. The dashed black lines are the approximations of Eqs. (5) and (6), and the red shaded region shows cutoff wave numbers spanning $\zeta = 2^{\pm 1/3}$ (see the text).

A small peak in the EPW heat capacity up to about $0.05k/e^-$ is present for temperatures kT just below the electron plasma wave energy $\hbar\omega_p$. At lower temperatures, the thermal energy is insufficient to excite these oscillations. At higher temperatures, the increasing Debye-Hückel screening length cuts off the shortest-wavelength modes that contribute most to the energy integral, resulting in a small negative heat capacity down to about $-0.002k/e^-$ as the energy remaining in these modes is released. The heat capacity at a given electron degeneracy also diminishes with increasing density, since E_F increases slightly faster with density than the EPW energy ($E_F \propto n^{2/3}$, $\hbar\omega_p \propto n^{1/2}$). At low temperature and density, hydrogen and many other materials recombine into neutral species, extinguishing the plasma oscillations.

Current hydrogen equation of state (EOS) models are sometimes grouped into "chemical" models that minimize the free energy of multiple chemical species (i.e., H_2, H_1, H_1^+, e^-) and "physical" models based on density functional theory and molecular dynamics or quantum Monte Carlo

(QMC) methods. Most wide-range theoretical EOS tables stitch different methods together depending on the thermodynamic conditions [28–33].

To make the difficult quantum calculations tractable in the WDM regime, only a small number of particles is included in the calculation and periodic boundary conditions are imposed [4,29,30]. These calculations are then naturally restricted to consideration of only short-wavelength (or high wave number) structures, often not even extending past the screening length λ_E, which is used here as the basis for the cutoff of the EPW integral. For example, a calculation with 64 atoms at a density corresponding to $E_F = 1$ Ry has a minimum wave number of 0.96 Å^{-1}, just barely reaching the cutoff (maximum) wave number of the plasmons at $kT = 1$ Ry (Fig. 2).

Finite-size corrections, when they are included, are commonly approximated using the static (zero frequency) limit, and recent studies [34] of dynamic finite-size effects have not evaluated the convergence to volumes larger than the EPW cutoff wavelength at thermodynamic conditions in the EPW active region predicted by this model.

Current hydrogen chemical EOS models and the analytic fits to physical models do not explicitly include a plasmon excitation term, and the finite-volume quantum calculations all have used too few particles to adequately treat even the shortest wavelength EPWs in the WDM regime [28–33].

A small missing energy term is consistent with recent experimental evidence that suggests hydrogen has additional internal energy compared to theoretical predictions in the WDM regime (Fig. 4). The highest-pressure deuterium shock measurements of Fernandez-Pañella *et al.* [5] above 300 GPa show additional compression (excess energy at the same pressure) compared to all theoretical models [28–33].

Compression of a material across a shock front is directly related to the change in internal energy through the Rankine-Hugoniot energy relation [20]

$$E_1 - E_0 = 0.5(P_1 + P_0)V_0(1 - 1/\eta), \tag{7}$$

where subscripts 0 and 1 correspond to the initial conditions and postshock state, respectively, and the compression ratio $\eta = \rho_1/\rho_0 = V_0/V_1$. The reported compression discrepancy corresponds to an internal energy bias of about 2% of $(E_1 - E_0)$ at the highest pressure (Fig. 4).

Shock compression of selected deuterium experiments and models is shown in Fig. 4(a). To illustrate the effect of additional plasmon internal energy contributions, Fig. 4(b) shows the same data as in Fig. 4(a) mapped to internal energy [20].

The magnitude and the trend of EPW internal energy, when added to the theoretical models, is sufficient to account for the additional internal energy observed in the experiments. The magnitude of the offset suggests that the cutoff wave number may be a bit higher than the inverse screening length, i.e., $\zeta \approx 2^{+1/3}$. Assuming this value of ζ,

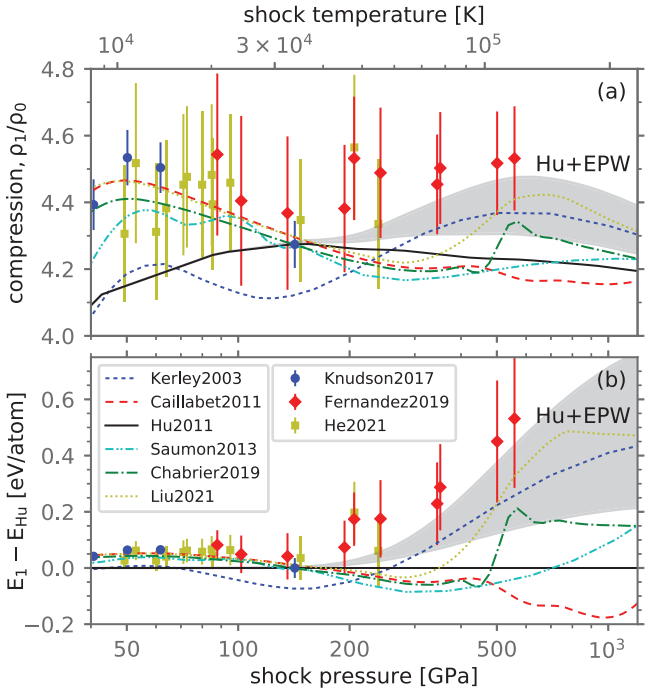

FIG. 4. Comparison of selected deuterium experiments [5,35,36] and theoretical EOS models [28–33] along the Hugoniot from a cryogenic liquid initial state. (a) Compression ratio. (b) Difference in internal energy of the data and models relative to Hu2011 [30]. The shaded band represents adjustment of the Hu2011 model with the addition of EPW energy using a range of cutoff multipliers $\zeta = 2^{\pm 1/3}$. Shocked deuterium is fully ionized above 50 GPa.

this model predicts that EPW internal energy has the maximum impact on shock compression of hydrogen near 700 GPa. Caution should be exercised when adding this EPW energy to larger quantum molecular dynamics calculations, so as not to double count energy contributions when wave numbers overlap with the EPW integral.

Some promising recent developments using Green's functions (GF) for the uniform electron gas [37,38] implicitly include EPW excitations. At conditions near the highest-pressure deuterium shock experiment, the GF method yields an energy 0.2 eV/e^- higher than a fit to QMC [37,39]; this magnitude is close to that of the present EPW model [Fig. 4(b)]. The GF method shows promise as a complementary approach to QMC, but currently no wide-range hydrogen EOS used for inertial fusion or astrophysical modeling deploys a GF calculation for the electron component.

Hydrogen is the primary constituent of most astrophysical bodies, including many that have some or most of their interiors in the WDM regime, such as low-mass main-sequence stars [40,41], substellar objects such as brown dwarfs and "hot" Jupiters [42], and the envelope of some white dwarfs [43]. An overlooked contribution to the specific heat will have implications for their structure

and evolution, particularly for those bodies with isentropic interiors that follow the EPW peak.

For example, specific heat is a key thermodynamic property that modifies if and where convection occurs, and a structural instability related to nonequilibrium ^{3}He fusion as stars transition from partly to fully convective interiors has been invoked to explain a spectral luminosity gap in low-mass main-sequence stars near $0.35M_\odot$ [44,45]. The equation of state in the interior has been identified as a plausible cause of the small quantitative offset of the simulated gap compared to observations [45], and the interior of these $0.35M_\odot$ objects is near the region where EPW internal energy is at its peak.

The hydrogen equation of state is a critical input to inertial confinement fusion ignition designs, where simulations using different EOS models can change the fusion yield by a factor of 2 and areal density by 50% [46]. Achieving high performance and reliability of ignition designs becomes more challenging if all current models are missing energy terms in the region where the cold hydrogenic fuel is being compressed (see Fig. 1). For current experiments right at the threshold of ignition [6,47], even small improvements to the precision of the design are amplified drastically in the implosion performance and reliability.

The results reported here have focused on the case of hydrogen, but this plasmon specific heat will emerge in plasmas of any composition. The modes of a plasma are like instruments in an orchestra, with tones of numerous instruments based on atomic, thermal, degeneracy, plasmon, and Coulomb coupling energies. Although the ensuing orchestra is not carried solely by the plasma notes, plasma oscillations do contribute to and enrich the overall symphony of substances in the warm-dense-matter regime.

The authors thank E. G. Blackman, G. Chabrier, S. X. Hu, V. V. Karasiev, A. L. Kritcher, and S. M. Rightley for useful feedback and discussions. This material is based upon work supported by the Department of Energy (DOE) National Nuclear Security Administration under Grant No. DE-NA0003856 and Office of Fusion Energy Sciences Grant No. DESC0019269, the University of Rochester, the New York State Energy Research and Development Authority, and National Science Foundation 19-528 Physics Frontier Centers, Grant No. 2020249, Center for Matter at Atomic Pressures. A portion of this work was performed at Lawrence Livermore National Laboratory under Contract No. DE-AC52-07NA27344.

*Corresponding author.
j.r.rygg@rochester.edu

[1] P. Debye, Zur theorie der spezifischen warmen, Ann. Phys. (Berlin) **39**, 789 (1912).
[2] J. W. Leachman, R. T. Jacobsen, S. Penoncello, and E. W. Lemmon, Fundamental equations of state for parahydrogen, normal hydrogen, and orthohydrogen, J. Phys. Chem. Ref. Data **38**, 721 (2009).
[3] A. Y. Potekhin and G. Chabrier, Thermodynamic functions of dense plasmas: Analytic approximations for astrophysical applications, Contrib. Plasma Phys. **50**, 82 (2010).
[4] T. Dornheim, S. Groth, and M. Bonitz, The uniform electron gas at warm dense matter conditions, Phys. Rep. **744**, 1 (2018).
[5] A. Fernandez-Pañella, M. Millot, D. E. Fratanduono, M. P. Desjarlais, S. Hamel, M. C. Marshall, D. J. Erskine, P. A. Sterne, S. Haan, T. R. Boehly, G. W. Collins, J. H. Eggert, and P. M. Celliers, Shock Compression of Liquid Deuterium up to 1 TPa, Phys. Rev. Lett. **122**, 255702 (2019).
[6] H. Abu-Shawareb *et al.*, Lawson Criterion for Ignition Exceeded in an Inertial Fusion Experiment, Phys. Rev. Lett. **129**, 075001 (2022).
[7] S. P. Regan, K. Falk, G. Gregori, P. B. Radha, S. X. Hu, T. R. Boehly, B. J. B. Crowley, S. H. Glenzer, O. L. Landen, D. O. Gericke, T. Doeppner, D. D. Meyerhofer, C. D. Murphy, T. C. Sangster, and J. Vorberger, Inelastic X-Ray Scattering from Shocked Liquid Deuterium, Phys. Rev. Lett. **109**, 265003 (2012).
[8] P. Davis, T. Doeppner, J. R. Rygg, C. Fortmann, L. Divol, A. Pak, L. Fletcher, A. Becker, B. Holst, P. Sperling, R. Redmer, M. P. Desjarlais, P. Celliers, G. W. Collins, O. Landen, R. W. Falcone, and S. H. Glenzer, X-ray scattering measurements of dissociation-induced metallization of dynamically compressed deuterium, Nat. Commun. **7**, 11189 (2016).
[9] S. Glenzer, O. Landen, P. Neumayer, R. Lee, K. Widmann, S. Pollaine, R. Wallace, G. Gregori, A. Höll, T. Bornath *et al.*, Observations of Plasmons in Warm Dense Matter, Phys. Rev. Lett. **98**, 065002 (2007).
[10] P. Sperling, E. Gamboa, H. Lee, H. Chung, E. Galtier, Y. Omarbakiyeva, H. Reinholz, G. Röpke, U. Zastrau, J. Hastings, L. Fletcher, and G. Glenzer, Free-Electron X-Ray Laser Measurements of Collisional-Damped Plasmons in Isochorically Heated Warm Dense Matter, Phys. Rev. Lett. **115**, 115001 (2015).
[11] B. B. Witte, L. Fletcher, E. Galtier, E. Gamboa, H. Lee, U. Zastrau, R. Redmer, S. Glenzer, and P. Sperling, Warm Dense Matter Demonstrating Non-Drude Conductivity from Observations of Nonlinear Plasmon Damping, Phys. Rev. Lett. **118**, 225001 (2017).
[12] D. Pines and J. R. Schrieffer, Approach to equilibrium of electrons, plasmons, and phonons in quantum and classical plasmas, Phys. Rev. **125**, 804 (1962).
[13] N. R. Arista and W. Brandt, Dielectric response of quantum plasmas in thermal equilibrium, Phys. Rev. A **29**, 1471 (1984).
[14] N. Maafa, Dispersion relation in a plasma with arbitrary degeneracy, Phys. Scr. **48**, 351 (1993).
[15] P. K. Shukla and B. Eliasson, Nonlinear aspects of quantum plasma physics, Phys. Usp. **53**, 51 (2010).
[16] D. B. Melrose and A. Mushtaq, Dispersion in a thermal plasma including arbitrary degeneracy and quantum recoil, Phys. Rev. E **82**, 056402 (2010).
[17] J. Daligault, Landau damping and the onset of particle trapping in quantum plasmas, Phys. Plasmas **21**, 040701 (2014).
[18] S. Rightley and D. Uzdensky, Landau damping of electrostatic waves in arbitrarily degenerate quantum plasmas, Phys. Plasmas **23**, 030702 (2016).

[19] An inverse definition for the degeneracy parameter is also common in the literature, i.e., where it is equal to the reduced temperature, $\theta_{\mathrm{alt}} = kT/E_F$. We choose the $\Theta = E_F/(kT)$ convention here such that a larger degeneracy parameter corresponds to higher degeneracy.

[20] See Supplemental Material at http://link.aps.org/supplemental/10.1103/PhysRevLett.130.225101 for more details on derivation of equations, EPW pressure contribution, EPW damping, relation between shock compression and energy, reanalysis of deuterium shock experiments, and comparison to other experiments, which includes Refs. [21–27].

[21] A. Einstein, Die plancksche theorie der strahlung und die theorie der spezifischen wärme, Ann. Phys. (Berlin) **327**, 180 (1907).

[22] M. P. Desjarlais, M. D. Knudson, and K. R. Cochrane, Extension of the hugoniot and analytical release model of alpha-quartz to 0.2–3 TPa, J. Appl. Phys. **122**, 035903 (2017).

[23] T. Sjostrom and S. Crockett, A liquid regime equation of state for silicon dioxide, AIP Conf. Proc. **1793**, 050010 (2017).

[24] M. C. Marshall, A. E. Lazicki, D. Erskine, R. A. London, D. E. Fratanduono, P. M. Celliers, J. H. Eggert, F. Coppari, D. C. Swift, P. A. Sterne, H. D. Whitley, and J. Nilsen, Developing quartz and molybdenum as impedance-matching standards in the 100-Mbar regime, Phys. Rev. B **99**, 174101 (2019).

[25] T. Boehly, D. Hicks, P. Celliers, T. Collins, R. Earley, J. Eggert, D. Jacobs-Perkins, S. Moon, E. Vianello, D. Meyerhofer, and G. Collins, Properties of fluid deuterium under double-shock compression to several mbar, Phys. Plasmas **11**, L49 (2004).

[26] D. Hicks, T. Boehly, P. Celliers, J. Eggert, S. Moon, D. Meyerhofer, and G. Collins, Laser-driven single shock compression of fluid deuterium from 45 to 220 GPa, Phys. Rev. B **79**, 014112 (2009).

[27] D. E. Fratanduono, M. Millot, A. Fernandez-Pañella, P. A. Sterne, G. W. Collins, D. G. Hicks, J. H. Eggert, T. R. Boehly, and P. M. Celliers, Measurement of the sound speed in dense fluid deuterium along the cryogenic liquid hugoniot, Phys. Plasmas **26**, 012710 (2019).

[28] G. Kerley, Equations of state for hydrogen and deuterium, Technical Report No. SAND2003-3613, Sandia National Laboratories, 2003, https://www.osti.gov/biblio/917468.

[29] L. Caillabet, S. Mazavet, and P. Loubeyre, Multiphase equation of state of hydrogen from *ab initio* calculations in the range 0.2 to 5 g/cc up to 10 eV, Phys. Rev. B **83**, 094101 (2011).

[30] S. X. Hu, B. Militzer, V. N. Goncharov, and S. Skupsky, First-principles equation-of-state table of deuterium for inertial confinement fusion applications, Phys. Rev. B **84**, 224109 (2011).

[31] D. Saumon, The SESAME 5267 equation of state of deuterium, Technical Report No. LA-UR-13-20032, Los Alamos National Laboratories, 2013.

[32] G. Chabrier, S. Mazevet, and F. Soubiran, A new equation of state for dense hydrogen–helium mixtures, Astrophys. J. **872**, 51 (2019).

[33] H. Liu, Q. Li, Q. Zhang, G. Zhang, H. Song, Y. Zhao, B. Sun, and H. Song, Progress on equation of state of hydrogen and deuterium, High Power Laser Part. Beams **33**, 012003 (2021).

[34] T. Dornheim and J. Vorberger, Finite-size effects in the reconstruction of dynamic properties from *ab initio* path integral Monte Carlo simulations, Phys. Rev. E **102**, 063301 (2020).

[35] M. D. Knudson and M. P. Desjarlais, High-Precision Shock Wave Measurements of Deuterium: Evaluation of Exchange-Correlation Functionals at the Molecular-to-Atomic Transition, Phys. Rev. Lett. **118**, 035501 (2017).

[36] Z. He, Q. Zhang, H. Liu, G. Jia, X. Huan, Z. Fang, Z. Xie, J. Ye, H. Shu, J. Dong, F. Zhang, Y. Tu, W. Wang, and S. Fu, High-precision equation of state benchmark for cryogenic liquid deuterium at ultrahigh pressure, Phys. Rev. B **103**, 134107 (2021).

[37] J. Kas, T. D. Blanton, and J. J. Rehr, Exchange-correlation contributions to the thermodynamic properties of the homogeneous electron gas from a cumulant green's function approach, Phys. Rev. B **100**, 195144 (2019).

[38] M. Laraia, C. Hansen, N. Shaffer, D. Saumon, D. Kilcrease, and C. Starrett, Real-space Green's functions for warm dense matter, High Energy Density Phys. **40**, 100940 (2021).

[39] V. V. Karasiev, T. Sjostrom, J. Dufty, and S. Trickey, Accurate Homogeneous Electron Gas Exchange-Correlation Free Energy for Local Spin-Density Calculations, Phys. Rev. Lett. **112**, 076403 (2014).

[40] G. Chabrier and I. Baraffe, Theory of low-mass stars and substellar objects, Annu. Rev. Astron. Astrophys. **38**, 337 (2000).

[41] I. Baraffe, D. Homeier, F. Allard, and G. Chabrier, New evolutionary models for pre-main sequence and main sequence low-mass stars down to the hydrogen-burning limit, Astron. Astrophys. **577**, A42 (2015).

[42] A. Burrows, W. B. Hubbard, J. I. Lunine, and J. Liebert, The theory of brown dwarfs and extrasolar giant planets, Rev. Mod. Phys. **73**, 719 (2001).

[43] D. Saumon, S. Blouin, and P.-E. Tremblay, Current challenges in the physics of white dwarf stars, Phys. Rep. **988**, 1 (2022).

[44] W.-C. Jao, T. J. Henry, D. R. Gies, and N. C. Hambly, A gap in the lower main sequence revealed by gaia data release 2, Astrophys. J. Lett. **861**, L11 (2018).

[45] G. A. Feiden, K. Skidmore, and W.-C. Jao, Gaia gaps and the physics of low-mass stars. I. The fully convective boundary, Astrophys. J. **907**, 53 (2021).

[46] S. X. Hu, V. N. Goncharov, T. R. Boehly, R. L. McCrory, S. Skupsky, L. A. Collins, J. D. Kress, and B. Militzer, Impact of first-principles properties of deuterium–tritium on inertial confinement fusion target designs, Phys. Plasmas **22**, 056304 (2015).

[47] O. Hurricane, D. Callahan, D. Casey, E. Dewald, T. Dittrich, T. Döppner, S. Haan, D. Hinkel, L. B. Hopkins, O. Jones *et al.*, Inertially confined fusion plasmas dominated by alpha-particle self-heating, Nat. Phys. **12**, 800 (2016).